

Cite this: DOI: 00.0000/xxxxxxxxxx

Received Date
Accepted Date

DOI: 00.0000/xxxxxxxxxx

Phase Separation Dynamics and Active Turbulence in a Binary Fluid Mixture

Sohail Ahmed, Zixiang Lin and Zijie Qu*

Active matter, encompassing natural systems, converts surrounding energy to sustain autonomous motion, exhibiting unique non-equilibrium behaviors such as active turbulence and motility-induced phase separation (MIPS). In this study, we present a novel two-fluids model considering dynamics of the Cahn–Hilliard (CH) model for phase separation with Beris–Edwards nematohydrodynamics equation for orientational order and two distinct momentum equations for active and passive fluids coupled by viscous drag. A phase field-based lattice Boltzmann method is used to investigate the existence of active turbulence and phase separation in the binary mixture. We analyze microphase separated domain under extensile and contractile stresses, long the statistical properties of turbulent flow. Key parameters, like active parameter, tumbling parameter and elastic constant, affect the characteristic scale of flow. Our findings show that the interaction of active stress and two-fluid hydrodynamics leads to complex non-equilibrium pattern formation. This offers insights into biological and synthetic active materials.

1 Introduction

Research on active fluids has expanded significantly in recent years, bridging fundamental aspects of non-equilibrium thermodynamics with applications to biology¹, space technology², and nano-medicine.³ These fluids, which range from biological examples such as bacterial swarms and cellular tissues to synthetic active colloids are complex fluids identified by the presence of an active phase whose individual units self-propel.^{4,5} Active fluids are prone to self-organization phenomena, thus developing correlated collective movements that can become spatio-temporally chaotic pattern, consisting of fluid jets and swirls referred to as active turbulence.^{6,7} Experimentally, this novel form of turbulence express itself to the low Reynolds number phenomenon.^{6,8} Contradictory to the classical turbulence of fluid, which occurs when fluid is driven by an external force and reaches it is nonequilibrium statistically steady state, active fluids are driven by microscopic constituents that transform chemical energy sources into kinetic energy.⁹ Continuum hydrodynamic models have been used to study the emergence of turbulence-like patterns.⁷ The kinetic energy spectrum of such turbulence in some theoretical models displays universal power-law behaviors depending on whether the wavenumber is greater or less than a typical vortex size.^{10,11} The k^{-4} scaling was successfully proved by early comparisons with computer simulations, while high-resolution Stokes flow numerical simulation later verified the k^{-1} power law.¹²

Various type of active fluids exist with varying length scales. Active nematic fluids¹³ are a particularly interesting type that contain highly elongated polar interacting units. Systems composed of vibrated monolayers of cylindrical rods,¹⁴ actin filaments,¹⁵ and certain types of bacteria¹⁶ suspended in a fluid layer are example of ANFs. As theory, computations, and experiments have all advanced at the same time, ANFs have recently attracted a lot of attention.¹⁷ Experiments have mostly been motivated by a desire to comprehend the physics of biological systems, and theoretical and computational advancements have mostly been made possible by closely adhering to the knowledge of passive liquid crystals.¹⁸ Among the classical models in the context of continuum mechanics for the description of nematic liquid crystals, the Beris–Edwards model is most comprehensive model in which the director field is replaced by a Q-tensor field¹⁹, thus allowing for a variable degree of order in the material. Many active nematic systems are currently studied using the Beris–Edwards model, which was first used in the study of liquid crystals. Reproducing the active turbulence seen in active nematic experiments has proven to highly successful.¹¹ Moreover, Assante *et al.*²⁰ noticed that coupling concentration and nematic ordering can lead to spontaneous microphase separation in inhomogeneous active nematics, and S. Bhattacharyya and J. M. Yeomans²¹ used a continuum theory to study active phase separation, driven by flows, in a mixture of an active nematic and a passive isotropic fluid.

Phase separation, a concept in physical chemistry, refers to dynamic processes where a homogeneous system spontaneously split into discrete phases with various compositions and physical

Global College, Shanghai Jiao Tong University, Shanghai 200240, People's Republic of China; E-mail: zijie.qu@sjtu.edu.cn

properties as a result of changes in external conditions and composition characteristics. Clifford *et al.*²² found in 2009 that RNA and protein-based granules in *Caenorhabditis elegans* embryos form droplets through phase separation. This gave rise to the idea of phase separation in biology, which describes how biomolecules such as proteins, lipids, and nucleic acids interact with one another through multiple bonds to form membrane-less organelles or bimolecular condensates in a uniform environment.²³ Motility-induced phase separation (MIPS) is one of the example of active phase separation, in which self-propelled particles can get trapped in highly dense region, forming a dense phase and a dilute phase.^{24,25} MIPS has been thoroughly investigated in both single-component systems and binary mixtures by theoretical and numerical approaches.^{26,27} Continuum models of active matter have been used to study the phase separation in active Brownian particles²⁸, cellular aggregate²⁹, self-propelled particles.³⁰ Some other representative studies where Cahn-Hilliard model used for the phase separation can be found in the works of Yin and Mihalev³¹, Speck³² and Saha *et al.*³³.

Based on the above review, it is worth mentioning here that many models have been carried out on different aspect of active fluids, however most of them treat the system as a single fluid with a concentration field or focus on turbulent dynamics of a single active phase,^{34,35} little attention was paid on the relative motion between active and passive components is essential for capturing phase ordering dynamics. The need of this work is to develop a comprehensive two fluid model that combines Cahn-Hilliard dynamics for phase separation with full nematohydrodynamics (Beris-Edwards equations) for orientational order and active stresses, while solving distinct momentum equations for each fluid coupled by viscous drag.³⁶ Using lattice Boltzmann simulations,^{37,38} we investigate how active turbulence and phase separation co-exist, examining microphase-separated domains under extensile and contractile stresses, statistical properties of turbulent flow including velocity and vorticity differences between fluids, and how key parameters activity coefficient ζ , tumbling and shear-aligning λ and nematic elastic constant K govern characteristic scales of turbulent flow.^{39,40} Our findings provide that the interplay between active stress and two-fluid hydrodynamics leads to rich non-equilibrium pattern formation, providing a more complete picture of how activity sculpts both structure and flow in biological and synthetic materials.

2 Model

We model a mixture of an active fluid and passive fluid. Each component has density, velocity and viscosity. The Cahn-Hilliards equation is considered to describe the phase separation dynamics, which is written as:^{36,41}

$$\frac{\partial \phi}{\partial t} + \nabla \cdot (\phi u_1) = M \nabla^2(\mu), \quad \mu = \frac{\delta \mathcal{F}}{\delta \phi}, \quad (1)$$

where ϕ is the concentration of active fluid, u_1 represents the velocity field of the active phase, and the non-negative mobility coefficient M is considered often as either a constant or a concentration-dependent variable. \mathcal{F} is the Landau-Ginzburg variation free-energy functional³⁶ and the chemical potential μ

is defined as the variational derivation of free energy functional with respect to ϕ as given in³⁶:

$$\mu = \frac{\delta \mathcal{F}}{\delta \phi} = f'(\phi) - \varepsilon^2 \nabla^2 \phi. \quad (2)$$

The interface thickness parameter ε is a key component of the Cahn-Hilliard equation, ensuring that the interface between different phases is smooth and well-defined. It plays a crucial role in regularizing the interface, controlling its width, and penalizing spatial variations in the concentration field. In the context of two phase flow, ε is essential for accurately modeling the complex dynamics of phase separation and concentration gradients, contributing to the overall understanding of active matter suspension behavior. And $f(\phi) = \phi^2(1-\phi)^2$ is the double-well potential, enforcing $\phi \in [0, 1]$. From the above equations we then write.^{36,41}

$$\frac{\partial \phi}{\partial t} + \nabla \cdot (\phi u_1) = M \nabla^2(f'(\phi) - \varepsilon^2 \nabla^2 \phi). \quad (3)$$

The microscopic momentum equations for each fluid is written as:

$$\phi \rho_1 \left(\frac{\partial u_1}{\partial t} + u_1 \cdot \nabla u_1 \right) = -\phi \nabla P_1 + \nabla \cdot (\phi \sigma_1) + F_{drag} + F_{active} + F_{ch}, \quad (4)$$

$$(1-\phi) \rho_2 \left(\frac{\partial u_2}{\partial t} + u_2 \cdot \nabla u_2 \right) = -(1-\phi) \nabla P_2 + \nabla \cdot ((1-\phi) \sigma_2) - F_{drag}, \quad (5)$$

where $(1-\phi)$ is the concentration of passive fluid and $u_{i=1,2}$, $P_{i=1,2}$, $\rho_{i=1,2}$, represent the velocity, pressure, density of each fluid respectively. For both component we have used a Newtonian viscous stress as defined by Yue *et al.*³⁶,

$$\sigma_{i=1,2} = \eta_{i=1,2} (\nabla u_{i=1,2} + \nabla u_{i=1,2}^T). \quad (6)$$

Clearly, the viscosity $\eta_{i=1,2}$ are considered different in this model. It is worthy to mention here that, for active nematic systems, due to considering the small sizes and velocities of microscopic particles, active stress dominated over elastic stress, as given in the work of Doostmohammadi *et al.*¹³ and Thampi *et al.*⁴². Based on the consider studies and following Saghatchi *et al.*⁴³, we employ a simplified stress formulation that neglects elastic stresses, as active stresses dominate the dynamics in high-activity regime. In this study, we have considered three forces namely, the drag force F_{drag} , active stress F_{active} and capillary stress F_{ch} related to active fluid and only drag force for the passive fluid. A viscous drag between the components of the fluids $F_{drag} = \gamma \phi (1-\phi)(u_2 - u_1)$, where γ is the momentum transfer coefficient between both fluids. The active stress for an active fluid system is known to take the form of $\zeta \mathbf{Q}$, with the prominent contribution to active stresses being proportional to the nematic tensor \mathbf{Q} . ζ is a phenomenological parameter that presents the activity strength in active fluids being negative for contractile systems, such as (bacteria pull, less common in bacterial suspensions) and positive for extensile systems (bacteria push along their orientation, typical for swimming bacteria like *Bacillus subtilis*). The factor ϕ ensures that this stress is localized to active phase, which form via phase separation (Cahn-Hilliard dynamics). The nematic tensor \mathbf{Q} captures

the anisotropy of bacterial motion, distinguishing active matter from isotropic fluids. The divergence $F_{active} = \nabla \cdot (\zeta \phi \mathbf{Q})$ translates this stress into a force that accelerates the velocity of the active phase u_1 , interacting with other forces such as drag and interfacial tension. And the nematic order parameter \mathbf{Q} is presented by a nematic tensor field as:

$$\mathbf{Q} = 2S(\mathbf{pp} - \frac{1}{2}\mathbf{I}). \quad (7)$$

Where, $0 \leq S \leq 1$ is the magnitude, \mathbf{pp} is the alignment axis of the nematic ordering, and \mathbf{I} is the identity matrix, ensuring that \mathbf{Q} is traceless and symmetric, characteristic of nematic liquid crystals. Apart from the active stress, due to an interface between two phases gives rise to another stresses in the flow field. To capture additional stresses, the back-coupling from the concentration of active phase ϕ to the fluid equation is inserted through capillary stresses.⁴⁴ It can be demonstrated by computing the capillary stress divergence that the associated force field reduces to^{36,44,45}

$$F_{ch} = \sigma_{CH} = -\mu \nabla \phi. \quad (8)$$

The dynamics nematic tensor \mathbf{Q} can be represented by the equation of nematodynamic¹³

$$\frac{\partial \mathbf{Q}}{\partial t} + \mathbf{u}_1 \cdot \nabla \mathbf{Q} = \mathbf{S}(\nabla \mathbf{u}_1, \mathbf{Q}) + \Gamma \mathbf{H}. \quad (9)$$

The equation is well known as Beris-Edwards equation, \mathbf{S} accounts for the response of the orientational order to the extensional and rotational components of the velocity gradient and is described for the nematic in¹³ as:

$$\begin{aligned} \mathbf{S}(\nabla \mathbf{u}_1, \mathbf{Q}) &= (\lambda \mathbf{E} + \Omega) \cdot (\mathbf{Q} + \frac{\mathbf{I}}{3}) + (\mathbf{Q} + \frac{\mathbf{I}}{3}) \cdot (\lambda \mathbf{E} - \Omega) \\ &\quad - 2\lambda(\mathbf{Q} + \frac{1}{3})(\mathbf{Q} : \nabla \mathbf{u}_1) \end{aligned} \quad (10)$$

where $\Omega = (\nabla \mathbf{u}_1 - (\nabla \mathbf{u}_1)^T)/2$ is the vorticity and $\mathbf{E} = (\nabla \mathbf{u}_1 + (\nabla \mathbf{u}_1)^T)/2$ is the rate of strain tensors. The relative dominance of the rate of strain and the vorticity in affecting the alignment of particles with the flow is characterized by the tumbling parameter λ . Mathematically, λ determines the character of objective time derivative of \mathbf{Q} . Γ is the rotational diffusion coefficient and $\Gamma \mathbf{H}$ is relaxational dynamics of the nematic tensor to the minimum of free energy and defined as

$$\mathbf{H} = -\frac{\delta \mathbf{F}}{\delta \mathbf{Q}} + (\mathbf{I}/3) Tr \frac{\delta \mathbf{F}}{\delta \mathbf{Q}}, \quad (11)$$

where Tr denotes the tensorial trace. The Helmholtz free energy¹³ is typically taken as:

$$\mathbf{F} = \frac{A}{2} \mathbf{Q}^2 + \frac{B}{3} \mathbf{Q}^3 + \frac{C}{4} \mathbf{Q}^4 + \frac{K}{2} |\nabla \mathbf{Q}|^2, \quad (12)$$

and the coefficients of this free energy, A, B, and C are material parameters, and the final term K is elastic constant.

3 Results and Discussion

We solve the governing equations in section 2 using a lattice Boltzmann method on a D2Q9 lattice model. Simulations are

performed for 1000 steps on a two-dimensional domain of size 256×256 with the periodic boundary conditions, where the space and time discretizations are chosen as $\Delta x = 1.0$ and $\Delta t = 0.1$ respectively. We use the following initial conditions fields:

$$u_1 = u_2 = 0, \phi = \phi_0 + \delta \phi_0 rand(x, y), \mathbf{Q}(x, y, t) = 0. \quad (13)$$

Here, $rand(x, y)$ is the random number generator between 0 and 1, and $\delta \phi_0 = 0.01$ is the small initial perturbation amplitude used to seed the phase separation dynamics. Further, the values of other physical parameters are selected as follow: the densities $\rho_1 = \rho_2 = 0.5$, the viscosities $\eta_1 = \eta_2 = 0.5$, the mobility coefficient $M = 0.1$, the interface thickness $\epsilon = 0.1$, the drag coefficient $\gamma = 0.1$, the nematic relaxation coefficient $\Gamma = 0.34$, the material parameters $A = 0.0$, $B = -0.3$, and $C = 0.3$, which we choose from Thampi *et al.*⁴⁶. Our analysis begins with a homogeneous mixture where the concentration of active phase is $\phi = 0.5$. A typical snapshot of the concentration profile at the final time, shown in Fig. 1, reveals a microphase-separated state with distinct regions of high and low concentration, indicative of MIPS. The root mean square (RMS) velocity u_{rms} and vorticity ω_{rms} , where vorticity $\omega = \nabla \times u$, are used to quantify the dynamics. Further, to check the validity and accuracy of the LBM method used here, we compare the spatial velocity correlation function obtained by our LBM simulations with those given by Thampi *et al.*⁴⁶ and very excellent agreement is found as shown in Fig.2. The spatial velocity correlation function is written as:

$$C_{vv} = \frac{\langle u(x) \cdot u(x+r) \rangle}{\langle |u(x)|^2 \rangle}. \quad (14)$$

The variation of $\Delta u_{rms} = u_{1rms} - u_{2rms}$ and $\Delta \omega_{rms} = \omega_{1rms} - \omega_{2rms}$

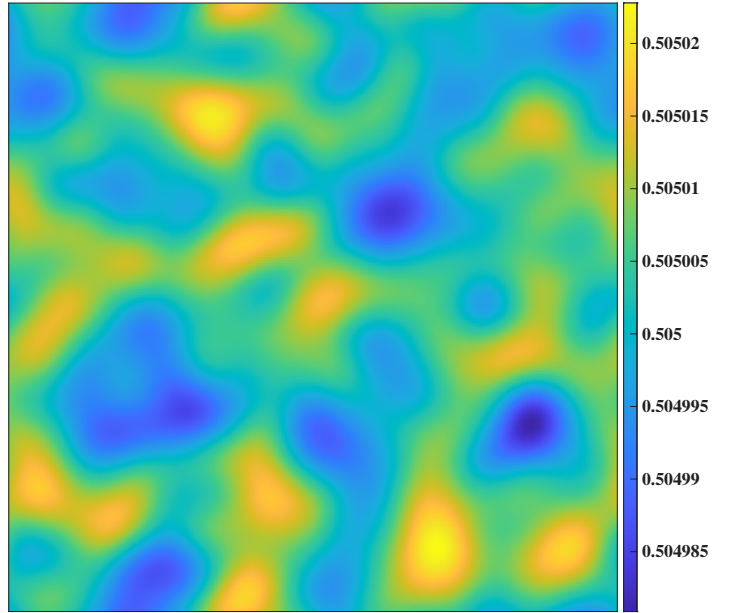


Fig. 1 Snapshot of the concentration profile in the microphase-separated state, color bar denotes the concentration of active phase.

as the function of active parameter ζ and concentration ϕ are depicted in Fig.3, respectively. It is observed from Fig. 3(a) and (b)

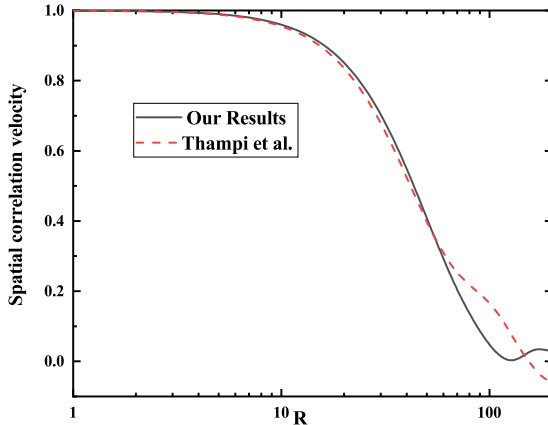


Fig. 2 Validation of our results with Thampi *et al.*⁴⁶, for spatial correlation velocity.

that increasing ζ from 0.05 to 0.1 leads to a significant increase in both the velocity difference Δu_{rms} and the vorticity difference $\Delta \omega_{rms}$. This enhancement occurs because a higher ζ amplifies the active stress ($\zeta \mathbf{Q}$), which injects more energy into the system and intensifies the turbulent flow. Furthermore, systems with a higher concentration of the active phase (ϕ) exhibit greater RMS values, as the active stress is localized to regions where ϕ is high, leading to more pronounced activity-driven fluctuations. Similarly, Fig. 4 represents the influence of varying elastic constant k on the root mean square velocity difference for both fluid, velocity difference of active fluid, vorticity difference of both fluid and vorticity difference in active fluid for the extensile and contractile values of active parameter. Fig.4 (a) and (b) demonstrate that larger K values (e.g., 0.3 and 0.8) reduce both Δu_{rms} and $\Delta \omega_{rms}$ compared to $K = 0.02$, suggesting that elastic effects decrease turbulent motion. Fig.4 (c) and (d) shows similar trends for u_{1rms} and ω_{1rms} , indicating that elastic contributions stabilize the active phase dynamics. Similarly to Fig.4, Fig.5 analyses the root mean square (RMS) velocity difference and RMS vorticity difference between both fluids in two different nematic alignment regimes, flow-tumbling and shearing-aligning. The figure clearly illustrates how the type of active stress (extensile vs. contractile) and the nematic alignment regime influence the turbulent dynamics and flow characteristics of the binary mixture. The flow kinematics and structural order for both contractile ($\zeta < 0$) and extensile ($\zeta > 0$) active parameter are thoroughly examined in Fig.6. Results for extensile system are shown by solid lines, whereas results for contractile systems are shown by dashed lines. Different colors are used to indicate the velocities u_1 , u_2 and their difference Δu , as well as nematic tensor \mathbf{Q} . We calculate the spatial and temporal velocity correlation functions in order to quantitatively examine the spatial coherence and temporal persistence of these flows. Eq. 14 provides the equation for the spatial velocity correlation function, and $Cvv(t)$, the temporal correlation that quantifies the

persistence of flow structure over time, is as follows:

$$Cvv(t) = \frac{\langle \mathbf{u}(\tau) \cdot \mathbf{u}(\tau+t) \rangle}{\langle |\mathbf{u}(\tau)|^2 \rangle}, \quad (15)$$

and the spatial correlation of the nemtaic order parameter, $C_{QQ}(r)$, measures the extent of orientational order:

$$C_{QQ}(r) = \langle Q(0) : Q(r) \rangle. \quad (16)$$

The spatial decay of velocity difference (Δu), the vorticity difference ($\Delta \omega$) and nematic correlation function are shown in Fig.6(a). With separate correlation profile for extensile ($\zeta = 0.1$) and contractile ($\zeta = -0.1$) stresses, a strong dependence on the active parameter ζ is observed, emphasizing how the direction of activity determines spatial ordering. According, the decay rates are closely related to the sign and magnitude of ζ , and the temporal correlations in Fig.6(b) show how these dynamics interactions change over time. These findings quantitatively demonstrate that the complicated collective behavior and phase separation dynamics in active turbulent states are mostly driven by activity.

Further, we characterize the energy of active nematic flows in the terms of isotropic kinetic energy spectra. We define the isotropic kinetic energy spectrum $E_{kin}(k)$ at isotropic wavenumber k , and following the work of Saghatchi *et al.*⁴³, the energy spectrum over the scalar wave number:

$$E_{kin}(k) = \frac{1}{2} \langle u_i(k) u_i(k) \rangle \quad (17)$$

Here $u_i(k)$ is the two dimensional Fourier transform of the velocity field, $k = \sqrt{k_x^2 + k_y^2}$ and $\langle \rangle$ denotes ensemble-averaging. In the classic turbulent flow for large Reynold number, a universal scaling was suggested by Andrei N. Kolmogorov⁴⁷ as $E_{kin}(k) \approx k^{-5/3}$, where $k = 2\pi/l_a$ is the wavenumber and l is the length scale. Active turbulence has been characterized through theoretical and experimental work as a low Reynolds number phenomenon. To determine the Reynolds number for our periodic nematics system, we consider the characteristic length scale as $L_a \approx \sqrt{K/\zeta}$ as suggested in⁴³. Combining this characteristic length with characteristic velocity scale of the flow, the mean square velocity velocity u_{1rms} and the other dimensional parameters such as Γ_1 , ρ_1 and η_1 provide a dimensionless Reynolds number as:

$$Re_1 = \frac{\rho_1 u_{1rms} L_a}{\eta_1}. \quad (18)$$

It should be noted that for passive fluid case we also consider numerically same characteristic length to calculate the Reynold number Re_2 for Γ_2 , ρ_2 and η_2 .

The kinetic energy spectra $E_{1kin}(k)$ of active fluid and $E_{2kin}(k)$ of passive fluid are plotted log-logically against wave number K at various values of active parameter $|\zeta|$ and phase concentration ϕ in Fig.7. At $\phi = 0.5$ and $\phi = 0.8$ respectively, panels (a) and (c) display the energy spectra of active fluid, whereas panels (b) and (d) display the energy spectra for passive fluid under the same circumstances.

The panels make it clear that the active exhibits a noticeable dependence of the active parameter ζ at low concentration ($\phi = 0.5$

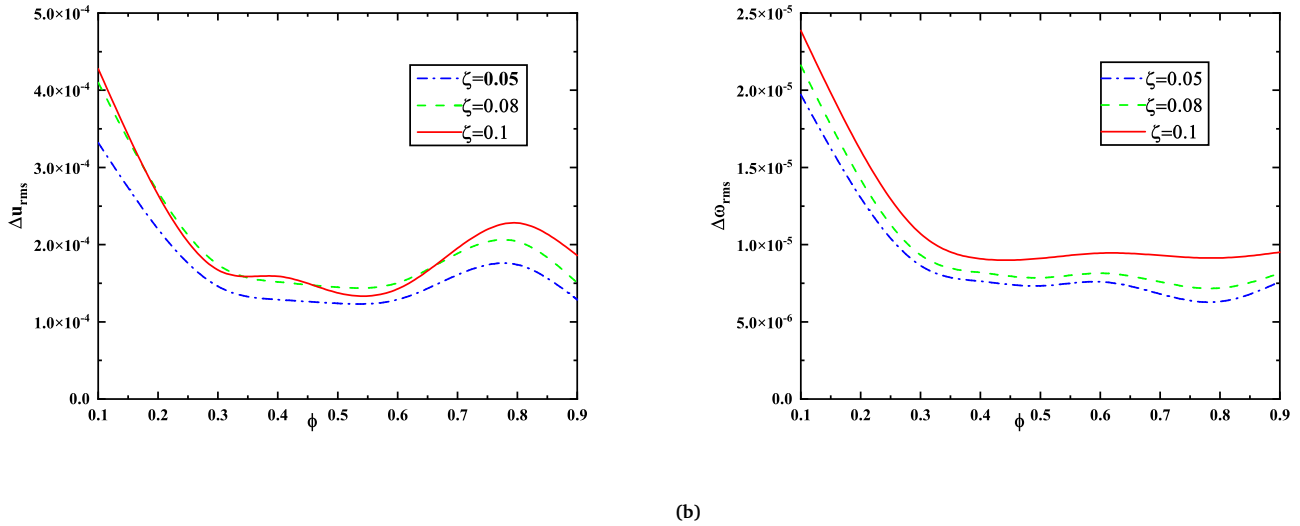


Fig. 3 Root mean square of velocity difference (Δu_{rms}) and root mean square of vorticity difference ($\Delta \omega_{rms}$) for different values of active parameter ζ and ϕ .

panel a). The overall energy level increases with larger value of $|\zeta|$, indicating a greater energy input into system as a result of stronger active stresses. Since the scaling differs from standard Kolmogorov⁴⁷ as $E(k) \approx k^{-5/3}$ because of the low Reynolds number regimes typical of active nematics, the spectra exhibit a power-law-like decay at intermediate wavenumbers, which is compatible with active turbulence. Viscosity drag effectively transfers momentum from the active phase to passive phase, as evidenced by the greater energy with higher $|\zeta|$ in the passive fluid spectrum (panel b).

The active and passive phases kinetic energy increases sufficiently at the higher active concentration value ($\phi = 0.8$ panels c and d) in comparison to the $\phi = 0.5$ case. This is obviously the case as the active fluid makes up a larger portion of the system. The active fluid (panel c) shows more pronounced energy across all wavenumbers, particularly at larger $|\zeta|$, where the system enters a stronger turbulent state. The passive fluid (panel d) also shows raised energy levels, but the relative difference between active and passive spectra narrows, suggesting more efficient coupling and energy sharing between the phase at high ϕ .

The Reynolds numbers Re_1 and Re_2 , calculated for each case and annotated in each panels, confirm that the system operates in low Reynolds number regime, characteristic of active turbulence. The increase in Re with $|\zeta|$ and ϕ further supports the visual and quantitative trends in the spectra.

Conclusions

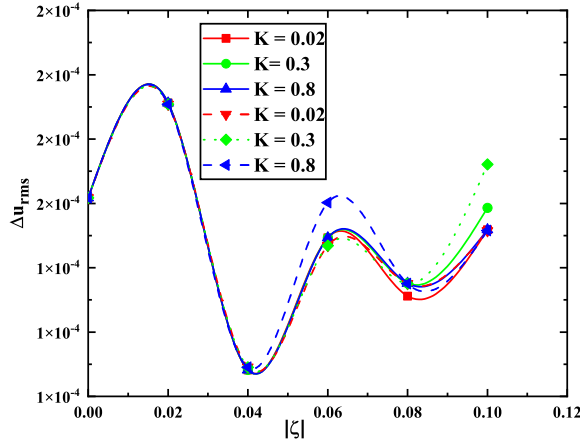
In this study, the two phase model for binary fluids mixture based on Cahn-Hilliard model for phase separation with the full Beris-Edwards nematohydrodynamics for orientational order has been developed. Different momentum equations considering different viscosity, density and concentration for each fluid and than coupled the momentum equation by viscous drag, the model provides

a detailed dynamics than single-fluid approaches for active fluid studies. The formation of a micro phase-separated pattern from homogeneous mixture has been recorded by apply lattice Boltzmann method, illustrating the phenomenon of MIPS within a turbulent active nematics. The model's validity was first confirmed by an excellent agreement with established spatial velocity correlation benchmarks for active turbulence³⁹. In summary, the main achievements are summarized as follow:

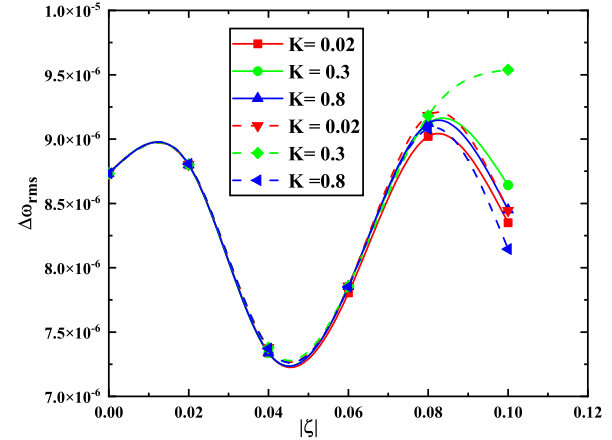
1- The larger values of active parameter $|\zeta|$ and active phase concentration ϕ , significantly enhances the velocity and vorticity differences between active and passive phases. Conversely, increasing the nematic elastic constant K suppresses these differences, indicating the stabilizing role of elastic forces.

2- the two-fluid nature of our system reveals crucial details about energy transfer. The kinetic energy of both phases increases with the activity strength $|\zeta|$, confirming that active stress is the primary energy source. The passive fluid spectrum also shows a k^{-4} decay, demonstrating that momentum is efficiently transferred from the active phase across a broad range of scales via viscous drag. At a higher active concentration ($\phi = 0.8$), the energy levels in both phases rise significantly and the spectra become more comparable, indicating enhanced coupling and energy sharing when the active phase percolates the system.

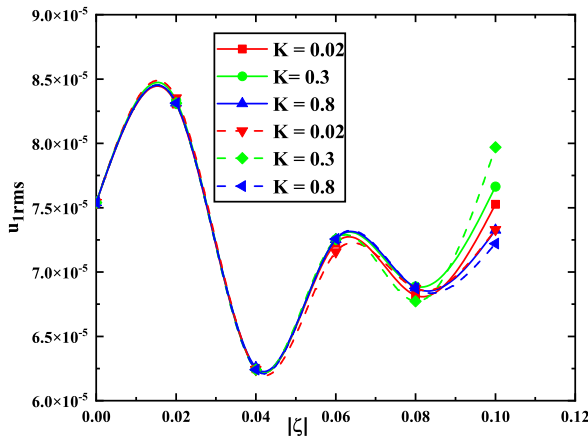
In summary, by combining the physics behind the phase separation, two fluid hydrodynamics, and active nematics, this work addresses relative motion and energy transfer in two fluids because of active parameter which has been neglected in previous studies. We have shown that the interaction between phase ordering with active stress-driven flow results in rich, non-equilibrium patterns in which the fluid components share energy from activity, forming the intricate flow fields as well as the structural domains. Our research provides a strong foundation for comprehending complex biological and synthetic active materials, where relative motion



(a)



(b)



(c)

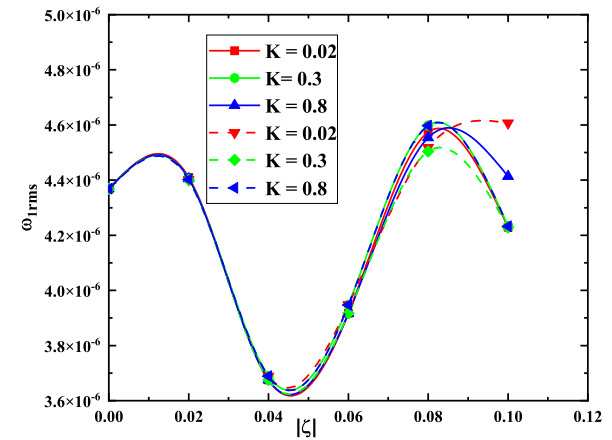
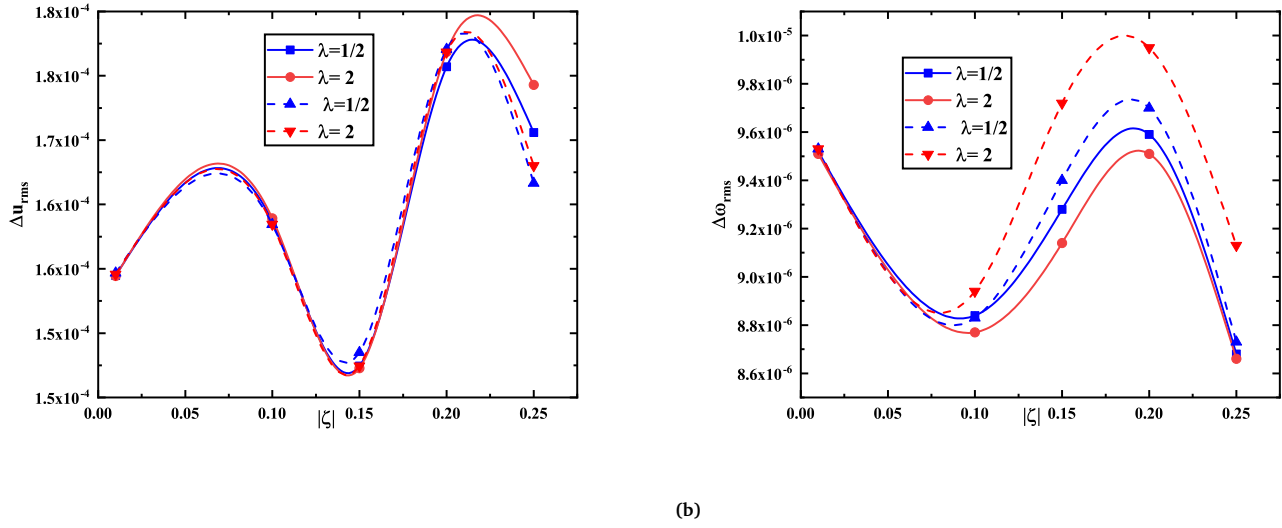


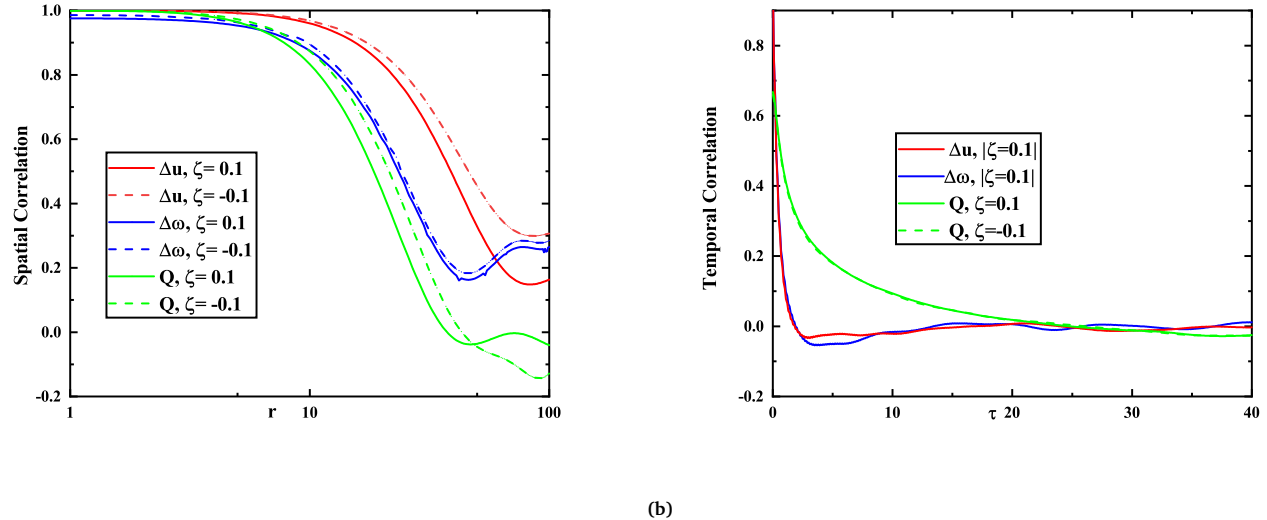
Fig. 4 Root mean square velocity and vorticity for different values of active parameter ζ (considering both extensile (solid lines) and contractile case (dashed lines)) and K . (a)- root mean square of velocity difference (Δu_{rms}), (b)- root mean square of vorticity difference ($\Delta \omega_{rms}$), (c)- root mean square of velocity for active phase (u_{1rms}), (d)- root mean square of vorticity for active phase (ω_{1rms}).



(a)

(b)

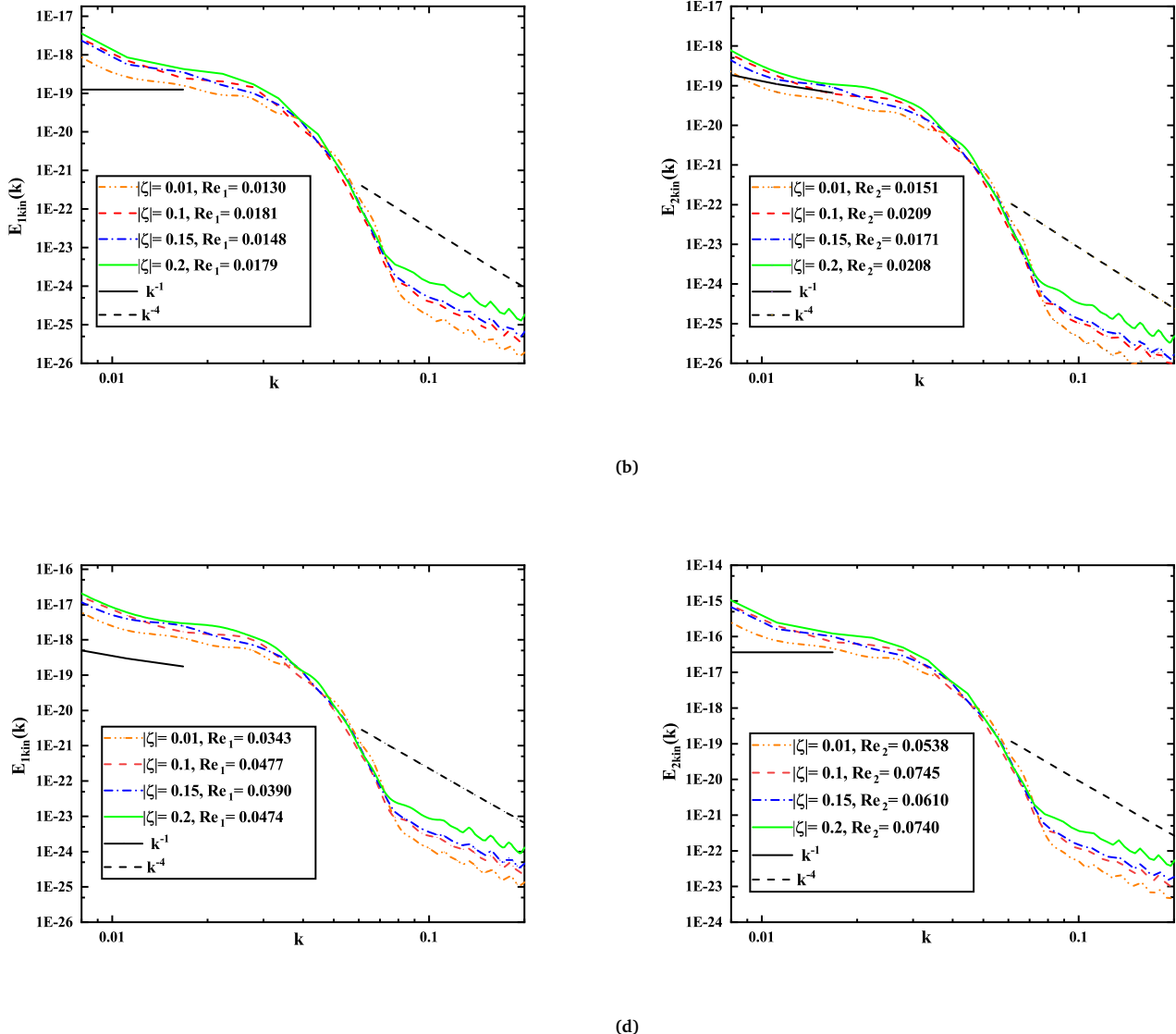
Fig. 5 Root mean square velocity and vorticity for different values of active parameter ζ (considering both extensile (solid lines) and contractile case (dash lines)) in both the flow-tumbling ($\lambda = 1/2$) and shear-aligning ($\lambda = 2$) regimes. (a)- root mean square of velocity difference (Δu_{rms}), (b)- root mean square of vorticity difference ($\Delta \omega_{rms}$).



(a)

(b)

Fig. 6 Correlation: (a) Spatial correlation, (b) temporal correlation, for the velocity difference of both phases (Δu), the vorticity difference of both phases ($\Delta \omega$) and nematic tensor Q for different values of active parameter ζ .



(c)

(d)

Fig. 7 Kinetic energy of active fluid (a) $\phi = 0.5$ and (c) $\phi = 0.8$ and base fluid (b) $\phi = 0.5$ and (d) $\phi = 0.8$ for different values of ζ (considering both extensile and contractile case) and Reynold number Re .

between components is important. Examples of these materials include bacterial colonies in polymeric solutions, cellular tissues with interstitial fluid, and active emulsions. Future research on the rheology of active mixtures, the behavior of topological defects in multi-phase systems, and the development of novel active soft materials will probably benefit significantly from this model, in our view.

Author contributions

Sohail Ahmed: Methodology, Conceptualization, Program coding, Mathematical and physical analysis, Writing, Investigation, Draft Preparation.

Zixiang Lin: Review and editing.

Zijie Qu: Supervision, Program checking, review and editing.

Conflicts of interest

The authors confirm that there is no any known financial or personal conflicts that would have appeared to have an impact on this research.

Data availability

The data that support the findings of this study are available from the corresponding author upon reasonable request.

Acknowledgements

We acknowledge the National Natural Science Foundation of China (NSFC) for the support our work through Grant No. 12202275.

Notes and references

- 1 F. Yang, S. Liu, H. J. Lee, R. Phillips and M. Thomson, *Nature Materials*, 2025, **24**, 615–625.
- 2 G. Volpe, C. Bechinger, F. Cichos, R. Golestanian, H. Löwen, M. Sperl and G. Volpe, *npj Microgravity*, 2022, **8**, 54.
- 3 A. Ghosh, W. Xu, N. Gupta and D. H. Gracias, *Nano Today*, 2020, **31**, 100836.
- 4 M. C. Marchetti, J. F. Joanny, S. Ramaswamy, T. B. Liverpool, J. Prost, M. Rao and R. A. Simha, *Rev. Mod. Phys.*, 2013, **85**, 1143–1189.
- 5 S. Ramaswamy, *Annual Review of Condensed Matter Physics*, 2010, **1**, 323–345.
- 6 H. H. Wensink, J. Dunkel, S. Heidenreich, K. Drescher, R. E. Goldstein, H. Löwen and J. M. Yeomans, *Proceedings of the National Academy of Sciences*, 2012, **109**, 14308–14313.
- 7 R. Alert, J. Casademunt and J.-F. Joanny, *Annual Review of Condensed Matter Physics*, 2022, **13**, 143–170.
- 8 C. Dombrowski, L. Cisneros, S. Chatkaew, R. E. Goldstein and J. O. Kessler, *Phys. Rev. Lett.*, 2004, **93**, 098103.
- 9 J. Dunkel, S. Heidenreich, K. Drescher, H. H. Wensink, M. Bär and R. E. Goldstein, *Phys. Rev. Lett.*, 2013, **110**, 228102.
- 10 S. Mukherjee, R. K. Singh, M. James and S. S. Ray, *Nature Physics*, 2023, **19**, 891–897.
- 11 L. Giomi, *Phys. Rev. X*, 2015, **5**, 031003.
- 12 R. Alert, J.-F. Joanny and J. Casademunt, *Nature Physics*, 2020, **16**, 682–688.
- 13 A. Doostmohammadi, J. Ignes-Mullol, J. Yeomans and F. Sagués, *Nature Communications*, 2018, **9**,
- 14 V. Narayan, S. Ramaswamy and N. Menon, *Science*, 2007, **317**, 105–108.
- 15 N. Kumar, R. Zhang, J. J. de Pablo and M. L. Gardel, *Science Advances*, 2018, **4**, eaat7779.
- 16 H. Li, X. qing Shi, M. Huang, X. Chen, M. Xiao, C. Liu, H. Chaté and H. P. Zhang, *Proceedings of the National Academy of Sciences*, 2019, **116**, 777–785.
- 17 A. Doostmohammadi and J. Yeomans, *The European Physical Journal Special Topics*, 2019, **227**, 2401–2411.
- 18 S. P. Thampi, *Current Opinion in Colloid and Interface Science*, 2022, **61**, 101613.
- 19 T. Qian and P. Sheng, *Phys. Rev. E*, 1998, **58**, 7475–7485.
- 20 R. Assante, D. Corbett, D. Marenduzzo and A. Morozov, *Soft Matter*, 2023, **19**, 189–198.
- 21 S. Bhattacharyya and J. M. Yeomans, *Phys. Rev. Lett.*, 2023, **130**, 238201.
- 22 C. P. Brangwynne, C. R. Eckmann, D. S. Courson, A. Rybarska, C. Hoege, J. Gharakhani, F. Jülicher and A. A. Hyman, *Science*, 2009, **324**, 1729–1732.
- 23 C. P. Brangwynne, T. J. Mitchison and A. A. Hyman, *Proceedings of the National Academy of Sciences*, 2011, **108**, 4334–4339.
- 24 M. E. Cates and J. Tailleur, *Annual Review of Condensed Matter Physics*, 2015, **6**, 219–244.
- 25 S. Mondal and P. Das, *Soft Matter*, 2025, **21**, 4093–4100.
- 26 R. Wittkowski, A. Tiribocchi, J. Stenhammar, R. J. Allen, D. Marenduzzo and M. E. Cates, *Nature Communications*, 2014, **5**, 4351.
- 27 H. Jeong, J. Gu, P. Mwasame, K. Patankar, D. Yu and C. E. Sing, *Soft Matter*, 2024, **20**, 681–692.
- 28 J. Stenhammar, A. Tiribocchi, R. J. Allen, D. Marenduzzo and M. E. Cates, *Phys. Rev. Lett.*, 2013, **111**, 145702.
- 29 H.-S. Kuan, W. Pönisch, F. Jülicher and V. Zaburdaev, *Phys. Rev. Lett.*, 2021, **126**, 018102.
- 30 A. Tiribocchi, R. Wittkowski, D. Marenduzzo and M. E. Cates, *Phys. Rev. Lett.*, 2015, **115**, 188302.
- 31 S. Yin and L. Mahadevan, *Phys. Rev. Lett.*, 2023, **131**, 148401.
- 32 T. Speck, J. Bialké, A. M. Menzel and H. Löwen, *Phys. Rev. Lett.*, 2014, **112**, 218304.
- 33 S. Saha, J. Agudo-Canalejo and R. Golestanian, *Phys. Rev. X*, 2020, **10**, 041009.
- 34 L. Giomi and A. DeSimone, *Phys. Rev. Lett.*, 2014, **112**, 147802.
- 35 M. L. Blow, S. P. Thampi and J. M. Yeomans, *Phys. Rev. Lett.*, 2014, **113**, 248303.
- 36 P. Yue, J. FENG, C. Liu and J. Shen, *Journal of Fluid Mechanics*, 2004, **515**, 293 – 317.
- 37 D. Marenduzzo, E. Orlandini, M. Cates and J. Yeomans, *Physical review. E, Statistical, nonlinear, and soft matter physics*, 2007, **76**, 031921.
- 38 C. Denniston, E. Orlandini and J. M. Yeomans, *Phys. Rev. E*, 2001, **63**, 056702.

- 39 S. P. Thampi, R. Golestanian and J. M. Yeomans, *Europhysics Letters*, 2014, **105**, 18001.
- 40 A. Doostmohammadi, M. F. Adamer, S. P. Thampi and J. M. Yeomans, *Nature Communications*, 2016, **7**, 10566.
- 41 A. Dadvand, M. Bagheri, N. Samkhaniani, H. Marschall and M. Wörner, *Physics of Fluids*, 2021, **33**, 053311.
- 42 S. P. Thampi, A. Doostmohammadi, R. Golestanian and J. M. Yeomans, *Europhysics Letters*, 2015, **112**, 28004.
- 43 R. Saghatchi, D. C. Kolukisa and M. Yildiz, *International Journal for Numerical Methods in Engineering*, 2023, **124**, 159–182.
- 44 M. E. Cates and E. Tjhung, *Journal of Fluid Mechanics*, 2018, **836**, P1.
- 45 R. Mueller and A. Doostmohammadi, *Phase field models of active matter*, 2021, <https://arxiv.org/abs/2102.05557>.
- 46 S. P. Thampi, R. Golestanian and J. M. Yeomans, *Philosophical transactions. Series A, Mathematical, physical, and engineering sciences*, 2014, **372**, 20130366.
- 47 A. N. Kolmogorov, *Proceedings of the Royal Society of London. Series A: Mathematical and Physical Sciences*, 1991, **434**, 9–13.